Tellus (2007), 59A, 80–95
Printed in Singapore. All rights reserved

TELLUS

Statistical properties of the temperature maxima in an intermediate order Quasi-Geostrophic model

By S. VANNITSEM*, *Institut Royal Météorologique de Belgique Avenue Circulaire, 3, 1180 Brussels, Belgium*

(Manuscript received 29 March 2006; in final form 28 August 2006)

ABSTRACT

The statistical properties of temperature maxima are investigated in a very long integration (2 400 000 months) of an intermediate order Quasi-Geostrophic model displaying deterministic chaos. The variations of the moments of the extreme value distributions as a function of the time window, n, are first explored and compared with the behaviours expected from the classical Generalized Extreme Value (GEV) theory. The analysis reveals a very slow convergence (if any) toward the asymptotic GEV distributions. This highlights the difficulty in assessing the parameters of the GEV distribution in the context of deterministic chaotic (bounded) atmospheric flows.

The properties of bivariate extremes located at different sites are then explored, with emphasis on their spatial dependences. Several measures are used indicating: (i) a complex dependence of the covariance between the extremes as a function of the time window; (ii) the presence of spatial (non-trivial) teleconnections for low-amplitude extremes and (iii) the progressive decrease of the spatial dependence as a function of the amplitude of the maxima. An interpretation of these different characteristics in terms of the internal dynamics of the model is advanced.

1. Introduction

Extreme events have a considerable impact on the societal activities, since they constitute situations that are far from the normal conditions under which the society and the biosphere are usually well adapted. These extreme events are by definition rare and the losses are expected to be quite limited over long time periods. However, climatic changes can considerably modify this view through the increase of the frequency of occurrence and the intensity of abnormal events (e.g. Kunkel et al., 1999; Sparks et al., 2002; Schär et al., 2004; Emanuel, 2005; Klein Tank et al., 2006; Elomer et al., 2006). This question is currently attracting most attention in the climate modelling community (see e.g. Kharin and Zwiers, 2000; Meehl et al., 2000; Bell et al., 2004; Beniston and Stephenson, 2004; Naveau et al., 2005).

One central difficulty when studying extreme events is obviously the lack of a large amount of natural data allowing for an exhaustive description of their statistical properties. This has led to the development of theoretical models, as well as techniques devoted to the statistical inference of their parameters. These tools constitute the classical extreme value theory (see e.g. Coles, 2001). It has been applied in many practical situations for which the return frequency of extreme events extracted from a rather short data set is necessary (e.g. Gumbel, 1958; Sneyers, 1979; Buishand, 1989).

One central hypothesis in this theory is the independence (or near-independence) of successive extreme events. However, a large class of systems governed by non-linear deterministic evolution laws display functional dependences that cannot enter in this category. Recently theoretical advances have been made for a subclass of such systems, known as chaotic maps (Balakrishnan et al., 1995). In particular, it has been shown that the probability distribution of the extremes is discontinuous even asymptotically, in deep contrast with the classical theory. These results highlight the important impact of the deterministic nature of the dynamics on the properties of the extremes.

Since the early development of atmospheric modelling, most efforts have been devoted to the development of models whose evolution equations are deterministic in nature. These systems have been proven to be very successful in describing and predicting the complex (apparently erratic) behaviour of the atmosphere. Although it does not preclude the possible presence of stochastic forcings that could influence the dynamics, it strongly suggests that the dominant (large-scale) part of the atmospheric dynamics can be described by deterministic laws, which display chaos for certain parameter values. A natural question is therefore to know what are the implications of the deterministic (chaotic) nature of the dynamics on the properties of the extremes in this system. Since there is currently no theory for continuous time deterministic systems, one is left to investigate

*Correspondence
e-mail: svn@oma.be
DOI: 10.1111/j.1600-0870.2006.00206.x

the properties of the extremes using the guidelines provided by the available theories but keeping in mind the above limitations. In the present paper, we investigate this question in the context of a realistic deterministic atmospheric model displaying spatio-temporal chaos, still sufficiently simple to allow for very long integrations.

In the traditional applications of the extreme value theory, one is usually interested in the univariate probability distributions of the extremes. Much less by the multivariate distributions, although a growing literature in the statitical journals exists on this topic (e.g. Coles, 2001). Two interesting applications of the bivariate theory in a meteorological context have been performed revealing its potentialities (Buishand, 1984; Beersma and Buishand, 2004). One particularly interesting aspect of the multivariate theory is to provide tools allowing for evaluating the spatial (or multivariate) dependences between the extreme values. This question is also investigated in the context of the quasi-geostrophic model.

In Section 2, some properties of the univariate probability distribution of the extremes expected from the classical extreme value theory are first reviewed, with emphasis on the convergence toward the asymptotic distributions known as the Generalized Extreme Value (GEV) distributions. In addition, a brief introduction to the multivariate case is provided with emphasis on the measure of bivariate dependences. Section 3 is devoted to the description of the atmospheric model and the long integration used in the present paper. The properties of the temperature maxima are then discussed in Sections 4 and 5. In the former an extensive analysis of the properties of the univariate probability distribution of the extremes as a function of the time window is performed, indicating their slow convergence toward the asymptotic universal laws. In the latter, spatial teleconnections between extremes are investigated using the measures of bivariate dependences presented in Section 2. Finally, the conclusions are given in Section 6.

2. The classical theory

2.1. Univariate probability distribution

Let us consider a random variable X_i recorded at a sample rate τ and the maximum of n consecutive events, M_n. The extreme value theorem states that under general continuity conditions and appropriate rescaling factors, a_n and b_n, the distribution of the maxima converges toward three universality classes known as the Fréchet (F), Gumbel (G) and Weibull (W) distributions,

$$\frac{M_n - b_n}{c_n} \to H_{F,G,W}. \tag{1}$$

These different distributions can be combined into a single family known as the Generalized Extreme Value (GEV) distribution,

$$\lim_{n\to\infty} \Pr((M_n - b_n)/a_n \le z) = G(z) = e^{-(1-\xi\frac{(z-\mu)}{\sigma})^{1/\xi}}, \tag{2}$$

where μ and σ are the asymptotic scale parameters and ξ the shape parameter of the distribution. Under a simple rescaling of the variables and in the limit of large n, one can write

$$Pr(M_n \le a_n z + b_n = z') = G'(z') = e^{-(1-\xi\frac{(z'-\alpha_n)}{\beta_n})^{1/\xi}}, \tag{3}$$

where $\beta_n = a_n\,\sigma$, $\alpha_n = b_n + a_n\,\mu$ and G' is a GEV distribution with different scale parameters.

If the distribution of the independent maxima, M_n, belongs to the Maximum Domain of Attraction (defined by the ensemble of distributions such that eq. (1) is valid) of one of the three universality classes, the distribution of the maxima, M_{nk}, for $k = 2,\ldots,\infty$ is also converging toward the same class with the same shape parameter but with different scale parameters (see Embrechts et al., 1997). The relations between the scale parameters of the two distributions can be deduced, by invoking the property of independence between the extremes for large value of n. Writing the probability distribution of the maxima, M_{nk}, as

$$\begin{aligned} Pr(M_{nk} \le z') &\approx G\left(\frac{(z'-\alpha_{nk})}{\beta_{nk}}\right) \\ &\approx G^k\left(\frac{(z'-\alpha_n)}{\beta_n}\right) \end{aligned} \tag{4}$$

and using the expression for the GEV distribution (for $\xi \neq 0$) and after some algebra, one gets

$$\beta_{nk} = k^{-\xi}\beta_n \tag{5}$$

$$\alpha_{nk} = \alpha_n - (k^{-\xi} - 1)(\beta_n/\xi). \tag{6}$$

Note that the domain of definition of these distributions are

$$\begin{aligned} &\text{for}\ \ \xi > 0,\ \ -\infty < z' < \alpha_n + \beta_n/\xi \\ &\text{for}\ \ \xi < 0,\ \ \alpha_n + \beta_n/\xi < z' < \infty \\ &\text{for}\ \ \xi = 0,\ \ -\infty < z' < \infty. \end{aligned} \tag{7}$$

The first, second and third moments of the GEV distribution can also be estimated and one gets (for $\xi \neq 0$),

$$\mu_n = \alpha_n + \frac{\beta_n}{\xi}(1 - \Gamma(1+\xi)). \tag{8}$$

$$\sigma_n^2 = \left(\frac{\beta_n}{\xi}\right)^2 (\Gamma(1+2\xi) - \Gamma(1+\xi)^2). \tag{9}$$

$$\alpha_n^3 = \frac{\beta_n^3}{\xi^3}(-\Gamma(1+3\xi) + 3\Gamma(1+\xi)\Gamma(1+2\xi) - 2\Gamma(1+\xi)^3). \tag{10}$$

where Γ is the gamma function. The skewness parameter, α_n^3/σ_n^3, can be derived

$$\gamma = \mathrm{Sign}(\xi)\frac{-\Gamma(1+3\xi) + 3\Gamma(1+\xi)\Gamma(1+2\xi) - 2\Gamma(1+\xi)^3}{(\Gamma(1+2\xi) - \Gamma(1+\xi)^2)^{3/2}} \tag{11}$$

and only depends on the shape parameter, ξ. The latter quantity suggests that if the distribution of extremes converges toward one of the universality classes (with $\xi \neq 0$), the skewness of the data should be asymptotically independent of an increase of the time

window n. Note that the value of γ for the Gumbel distribution is 1.1396 (Gumbel, 1958).

It is also worth mentioning that under the hypothesis that the distribution of the maxima has reached an asymptotic GEV family (with $\xi \neq 0$), the variance of the distribution should vary as

$$\sigma_{nk}^2 = k^{-2\xi}\sigma_n^2 \tag{12}$$

indicating a monotonic power law decrease or increase of the variance as a function of the time window depending on the sign of ξ.

The properties described above are valid asymptotically, but the rate of convergence toward one of the asymptotic GEV distributions depends crucially on the nature and the distribution of the underlying process. For instance, for an independent identically distributed (iid) Gaussian variable, the convergence is very slow, and much faster for an iid process whose distribution is exponential. This has led some authors to propose transformations of the data in order to improve the speed of convergence (see e.g. Van den Brink et al., 2004, and references therein).

This theory, developed in the context of iid processes, has been successfully extended to stationary processes displaying short term dependences (see e.g. Coles, 2001). However, for atmospheric and climate problems, the different assumptions underlying the development of this wonderful theory are difficult to meet since these systems experience complex variations on a wide range of space and time scales far from the iid or short term dependent processes. Similar features are also present in deterministic models that have been used successfully to describe the dynamics of the atmosphere and climate.

One of the principal signature of these models (shared with the atmosphere) is the property of sensitivity to initial conditions whose origin can be traced back to their chaotic dynamics. Concomitantly, they display an erratic behaviour with strong similarities with the atmospheric dynamics and which is, most of the time, hardly distinguishable from a random process. In view of the erratic character of their solutions, this type of systems are often investigated using a probabilistic approach. Still, the deterministic nature of the process introduces a functional dependence for all times and little is known concerning the asymptotic properties of the extremes in such systems. One very interesting work in this context has been done by Balakrishnan et al. (1995) in which asymptotic properties of the extremes in chaotic maps (discrete time chaotic systems) have been deduced analytically and numerically. In particular, they showed on some typical maps that the extreme value distribution does not converge toward one of the universality classes and that this distribution is discontinuous. Furthermore, they have associated these features with the periodic orbits embedded in these systems.

Although the basic assumptions of the classical extreme value theory are not, strictly speaking, applicable in the context of a deterministic system, one natural question is to know what are the limitations of the use of the GEV theory for such systems since their dynamics bear strong resemblance to the natural one. This will be the central topic of Section 4.

2.2. Multivariate theory

Up to now, some aspects of the classical theory for a single variable have been discussed. A theory has also been developed for multivariate processes (Coles, 2001, for a review), and in particular for bivariate processes. In the latter case, limit theorem exists but the possible limit classes are much wider than for the univariate probability distribution. One popular class currently used is the "logistic" family for which an additional parameter now appears characterizing the interdependence between the two variables under considerations. This interdependence is the central information necessary to select one specific logistic distribution (see Buishand, 1984; Coles, 2001; Beersma and Buishand, 2004).

To measure this interdependence several approaches have already been used. Buishand (1984) proposes to write the joint distribution as

$$G(x, y) = (F(x)K(y))^{\theta(x,y)}, \tag{13}$$

where $F(x)$ and $K(y)$ are the univariate (or marginal) distributions of the variables x and y, respectively, and $\theta(x, y)$ characterizes the distance from independence. For $\theta(x, y) = 1$, the variables are independent and for $\theta(x, y) = 0.5$ (and under the hypothesis that the two marginal distributions are identical), the dependence is full. In principle, this quantity should be checked for all pairs of thresholds x and y.

One natural way to evaluate the spatial dependence is to fix the same threshold value $x = y$, assuming that the impact of the extremes is the same at every location. This aspect will be investigated in Section 5. However in a world in which the biosphere is well adapted to its own local environment, a specific threshold value could be felt as either an extreme or a normal event. In order to evaluate the impact of extreme situations at both locations, one must consider events that are indeed occurring in the tail of the probability density of the respective variables. In other words, one has to analyse threshold values that correspond to quantiles of the marginal distributions. This aspect is analysed using a second measure of dependence presented below. This measure has the advantage to be independent of the marginal distributions (Coles et al., 1999; Coles, 2001). It is based on a function, C, known as the copula which relates the marginal distributions and the multivariate distribution as (see Favre et al., 2004, for a detailed discussion of this quantity)

$$\begin{aligned} C(F_1(x_1), F_2(x_2), \ldots, F_n(x_n)) &= F(x_1, x_2, \ldots, x_n) \\ &= F(X_1 \leq x_1; \ldots; X_n \leq x_n) \end{aligned} \tag{14}$$

If the marginal distributions are continuous, this function C is unique. It can be obtained through a change of variables from $x_1, \ldots x_n$ to the new variables $U_1 = F_1(x_1), \ldots, U_n = F_n(x_n)$.

C is the multivariate distribution of the variables, $U_1, \ldots, U_n$. For independent variables, it reduces to the product of marginal distributions, $C(U_1, \ldots, U_n) = U_1 \ldots, U_n$. The new variables $\{U_i\}$ are uniformly distributed between 0 and 1. In the present paper, we focus on the bivariate distributions since they already provide important information on the spatial dependences.

Instead of looking at the properties of the original variables, the properties of the new variables defined by the empirical marginal distributions as

$$u_i = F_x(x_i) = \frac{\#x_j \leq x_i}{N+1}$$
$$v_i = F_y(y_i) = \frac{\#y_j \leq y_i}{N+1}. \tag{15}$$

are explained. To evaluate the dependence for this bivariate process, Coles et al. (1999) propose a measure of the form

$$\xi(u) = 2 - \frac{\ln \Pr(U \leq u, V \leq u)}{\ln \Pr(U \leq u)}. \tag{16}$$

For independent variables, $\xi(u) = 0$, and for full dependence, $\xi(u) = 1$. In contrast with the approach proposed in eq. (13), this measure characterizes the dependence of the variables for the same quantile value, u, of the marginal distributions. Both measures will be used on the data presented in the next section.

3. Experimental settings

As indicated in the Introduction, one difficulty in assessing the properties of the extremes in natural time series is their sparse occurrence. An exhaustive analyses of the properties of these extremes can only be made for simple systems for which analytical relations can be deduced or for which very long synthetic runs can be produced. The latter approach is adopted here in the context of a Quasi-Geostrophic model still sufficiently simple to allow for extensive integrations. A similar approach has already been adopted in Van den Brink et al. (2004) to infer the role of climatic changes on the marginal distribution of the annual wind extreme events in the context of a coupled Ocean-Atmosphere model whose atmospheric component is basically the same as the model used in the present study. The advantage of using the atmospheric part only is its faster integration.

The model describes the evolution of the potential vorticity at 200, 500 and 800 hPa (Marshall and Molteni, 1993). The horizontal fields Z are expanded in series of spherical harmonics $Y_{m,n}$ truncated triangularly at wavenumber 21:

$$Z(\lambda, \phi, t) = \sum_{n=0}^{21} \sum_{m=-n}^{m=n} Z_{m,n}(t) Y_{m,n}(\lambda, \phi). \tag{17}$$

where λ, ϕ, m and n are the longitude, the latitude, the zonal and total wavenumbers, respectively. The index n represents a total (two-dimensional) wavenumber on the sphere and characterizes the size of the two-dimensional horizontal structures. The prognostic equation at each level, i, can then be written in terms of the streamfunction ψ and the potential vorticity q as

$$\frac{\partial q_i}{\partial t} = -J(\psi_i, q_i) - D(\psi_i) + S_i \tag{18}$$

where J is the jacobian of the two-dimensional field. The linear term D accounts for the effects of Newtonian relaxation of temperature, a scale selective horizontal diffusion of vorticity and temperature and a drag on the 800 hPa wind whose coefficient depends on the properties of the underlying surface. The damping timescale τ_d at total wavenumber 21 associated to the horizontal diffusion was fixed in Marshall and Molteni (1993) to 2 d. Finally the time-independent spatially varying source term, S, constrains the solution of the model to an averaged, statistically stable, observed winter climatology ("perpetual winter" conditions). This source term has been computed from observed winter streamfunction fields archived at the European Center of Medium Range Weather Forecasting (January and February 1984–1989). The way this source term is built can be found in Marshall and Molteni (1993).

Note that all the fields are computed in non-dimensional units: the length unit is the earth radius (6371 km) and the time unit is half the inverse of the angular velocity of the earth ($7.292\ 10^{-5}$ s^{-1}). The model equations are integrated in time using a leapfrog scheme for the Jacobian term, J, and a forward scheme for the linear operator, D, with a time step of 1 hr. The dynamics of this model has been investigated in details in Vannitsem and Nicolis (1997). It was shown that the solution of model (18) is chaotic and lives on a high-dimensional attractor.

Clearly, this model has many limitations like the absence of seasonal and daily periodicities, the absence of a water cycle, the use of simplifying assumptions like the hydrostatic approximation and the geostrophic relation. However as shown in Marshall and Molteni (1993) this model displays statistical and dynamical properties which are very close to the ones of the large scales of the atmosphere during winter in the Northern Hemisphere.

For our analysis, different variables can be considered in this model: wind, geopotential or temperature. In view of the central role played by the temperature in the climate change problem, we focus on the temperature field, written as

$$T = -\frac{p f_0}{R} \frac{\partial \psi}{\partial p}, \tag{19}$$

where p denotes the pressure, R, the gas constant, and f_0 the coriolis parameter at middle latitudes. Since the streamfunction field is defined at three levels, (vertically averaged) temperature fields can only be defined for the two layers 200–500 and 500–800 hPa. In the following the temperature defined in these two layers will be referred as the 350 and 650 hPa level temperature fields, respectively.

Note that in our idealized atmosphere, there is no particular interest in working with the minima or the maxima (as it could be the case when working with real data). So we are presenting here results obtained with the maxima, although the minima display similar properties of convergence and spatial dependences.

A data set of 2 400 000 months is used, based on 10 integrations of 240 000 months each starting from different initial conditions on the attractor of the system. The temperature maxima for a range of windows from 1 d up to 600 months have been recorded on a Gaussian grid corresponding to the T21 truncation of the model for 216 grid points over a latitudinal band from 30° North up to 53° North, with a higher concentration over North America, the Atlantic and Europe. This latitudinal band has been selected because the model is designed to provide a realistic winter climatology at middle latitude in the Northern Hemisphere (see Marshall and Molteni, 1993). For a window of $n = 600$ months, we have still 4000 maxima at each location.

4. The univariate distributions of the extremes in the QG model

One central hypothesis made in most of the practical applications of the analyses of the extreme events is the independence in space and time for large time windows. At the level of the time-correlation this assumption is quite reasonable. In the present model, this quantity has been computed and found to be close to 0 for windows beyond a few months. However, it is well known that this linear correlation analysis does not provide a proof of the strict independence between events. For a non-linear deterministic system such as the one studied here, a functional dependence always relates these events. In this sense, the system displays an infinite memory.

4.1. The moments of the extremes

In the classical theory, the probability densities of extremes are continuous functions of the variables. This continuity has been found to be absent in the context of (low-order) chaotic maps (Balakrishnan et al., 1995), property that has been associated with the deterministic nature of the dynamics. In the present model, the probability densities of extremes have been computed and found to be reasonably smooth except at some particular points and for particular time windows as illustrated in Fig. 1 which displays the probability density at one grid point (47°N, 135°E) of the QG model at 350 hPa. In the top panel (Fig. 1a), the distribution for different time windows is displayed. As expected, the distribution is shifted towards larger values for increasing n, but the most interesting feature is the appearance of small amplitude multiple peaks for large values of n, which seems to be robust against the change of the number of events used to build the distribution (Fig. 1b).

The presence of these peaks suggests that the probability density may be discontinuous as expected from the analysis of Balakrishnan et al. (1995). However, an important difference with the latter work lies in the fact that this discontinuity is not visible for small windows.

Now one could still expect that the probability distributions of the extremes can be approximately described by one

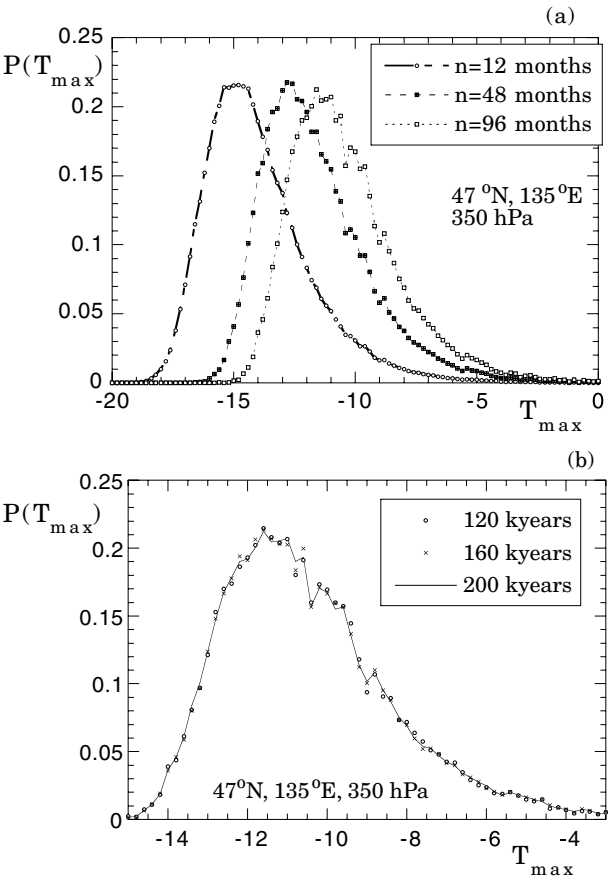

Fig. 1. Probability density of the temperature maxima at one grid point (47°N, 135°E) at 350 hPa for (a) different time windows using 2 400 000 months, (b) $n = 96$ months using three time-series lengths.

of the three universality classes and to get a distribution for which the parameter ξ is asymptotically independent of the time window n.

Note that from a dynamical point of view, the extreme values are bounded because of the finite size of the attractor of the system. One therefore expect that the value of ξ be positive. If it is not the case, one should either conclude that the estimated value is not correct or that there is no attractor for our system. Since there is no reason to believe that the solution generated by the model is only a transient behaviour towards infinity, one should conclude that the parameter ξ should be positive.

Let us therefore compute the skewness parameter (having a one-to-one correspondence with the value of ξ) for different time windows. Figure 2 shows the result for different grid points at the two levels at which the temperature is defined for 47° North. The skewness for 650 hPa is increasing as a function of the time window, with an apparent convergence towards a plateau. This behaviour first suggests that the asymptotic distribution is not reached yet for windows between 12 and 120 months. It is also interesting to note that the value at 135°E for a window of 600 months is larger but close to the value corresponding to the

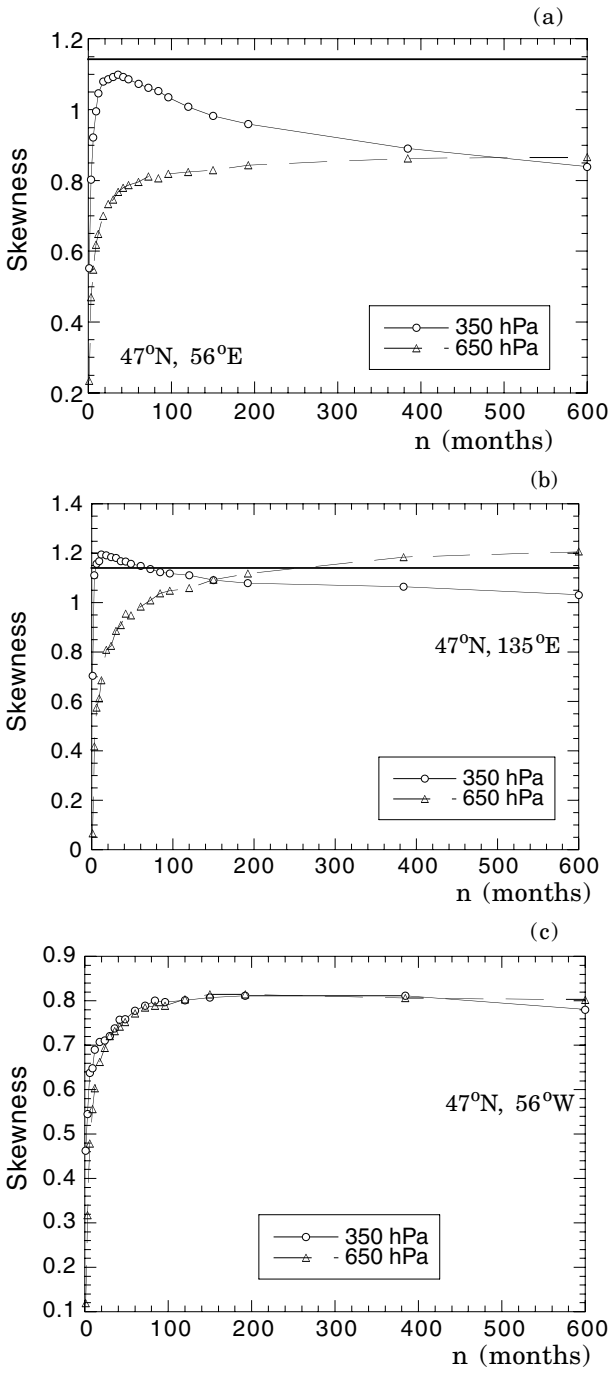

Fig. 2. Convergence of the skewness parameter, γ, as a function of the time window, n, at different grid points along the parallel located at 47° North, (a) 56°E, (b) 135°E and (c) 56°W. The straight lines refer to the parameter γ of the Gumbel distribution.

Gumbel distribution (1.1396). This marginal value cannot however be used to state that the shape parameter is indeed smaller than 0 since the number of extreme events is getting smaller with the size of the window.

At 350 hPa, the behaviour is slightly different with an overshoot around $n = 12$ months for grid points 56°E and 135°E, reaching for the latter a value of γ larger than the one associated with the gumbel distribution (1.1396). This indicates that for increasing time windows γ can reach values corresponding to positive values, negative values and finally to positive values again for ξ. So clearly depending on the time window, the nature of the extremes can be falsly interpreted as pertaining to a Fréchet distribution.

This convergence is similar at other latitudes as illustrated in Fig. 3 for grid points at 30° North, except that there is no overshoot for these low latitudes and the values do not exceed the gumbel value of 1.1396. For higher latitudes, the skewness parameter can sometimes reach large values as for grid points located close to 53°N, 135°E as can be seen on Fig. 7c, suggesting that the temperature in this region is falling into the Fréchet family distribution for large windows (ξ negative).

One limitation of the use of the skewness parameter is that its estimation is highly variable and biased in small samples (i.e. here for large time windows). One can therefore wonder whether our results above are reliable. In order to check that we have computed direclty the GEV parameters based on the L-moments that are known to be almost unbiased and much less sensitive to large values (see e.g. Stedinger et al., 1993). Fig. 4 displays the results for the same grid points as in Fig. 2. The variation of the shape parameter reveals further the slow convergence towards a plateau after about 120–240 months depending on the grid point considered. For reference, we have also drawn the 95% error bars that are obtained when assuming that the extreme events are independent. In addition we have performed a second integration of 2 400 000 months, referred in the figures as the second series. Most of the time, this second estimate lies within the error bars.

Note that the values of the shape parameter that can be inferred from the computation of the skewness parameter is close to the one obtained from the L-moment technique. For grid point located at 47°N 135°E, it is interesting to note that at 350 hPa the shape parameter is negative for short time windows as expected from the evolution of the skewness parameter. For long time window, the shape parameter is close to 0 for both levels in agreement with the proximity of the skewness parameter to the Gumbel value. For grid points located around 53°N, 135°E, the shape parameter computed with the L-moment technique is definitely negative (at the 95% confidence level) for intermediate and large windows (not shown).

To evaluate the spatial properties of the moments of the extremes, we have plotted the variance and the skewness for different time windows, n, for three latitudes, 30°, 47° and 53° North and for longitudinal grid points separated by about 28 degrees.

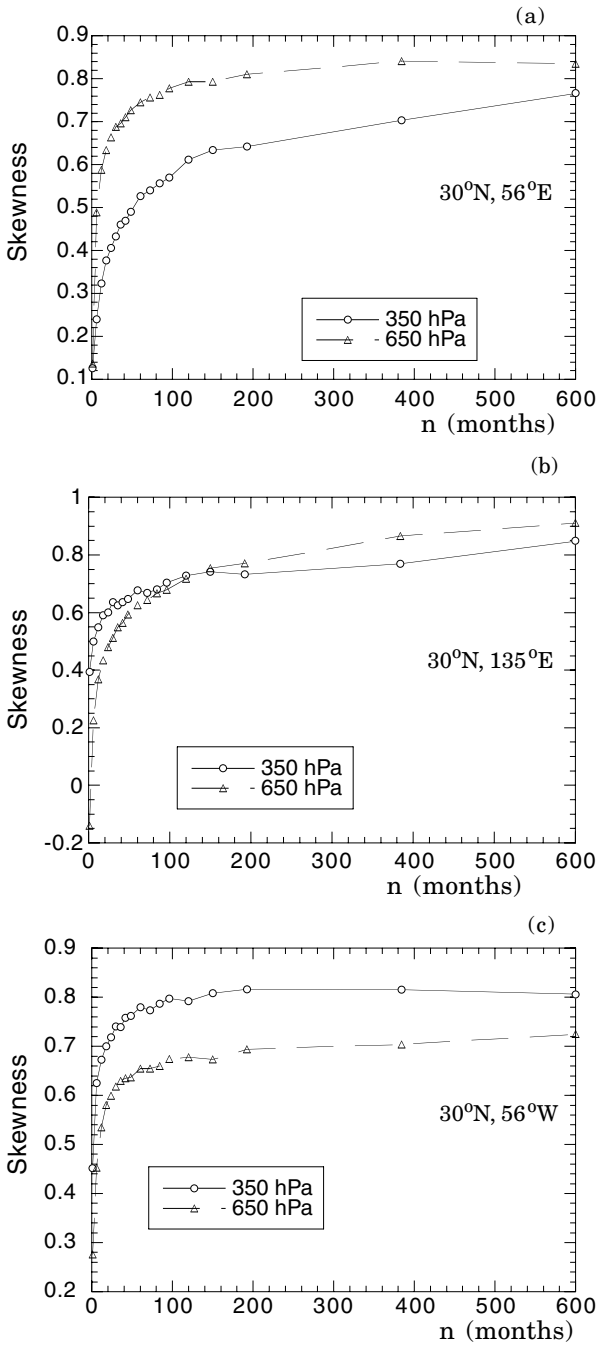

Fig. 3. As in Fig. 2 but along the parallel located at 30° North.

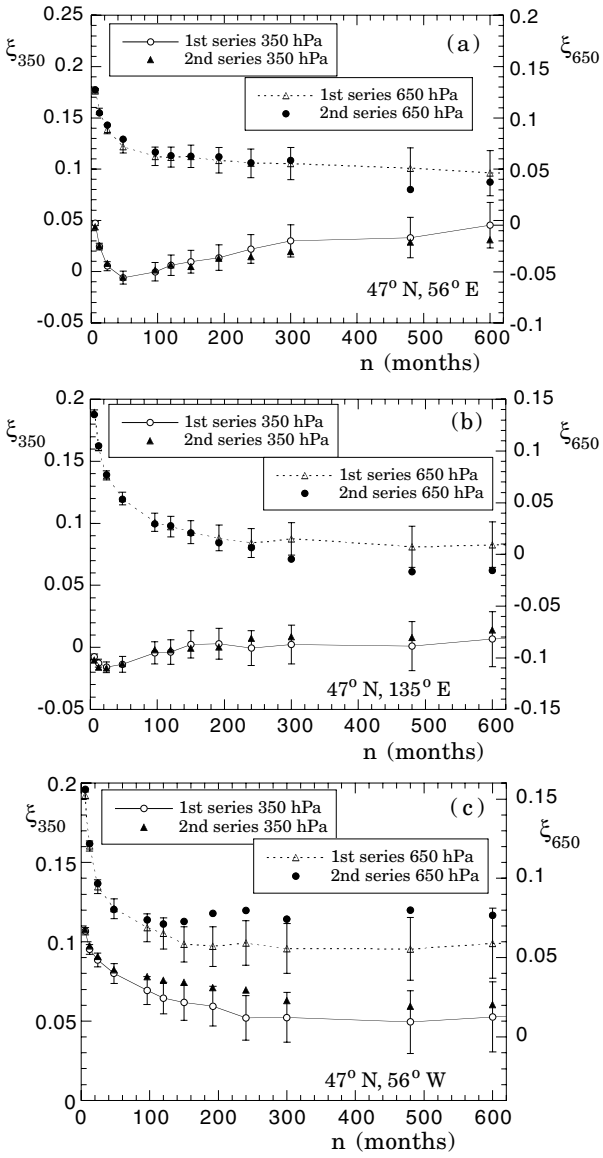

Fig. 4. Convergence of the shape parameter of the GEV fit as a function of the time window, n, at different grid points along the parallel located at 47° North, (a) 56°E, (b) 135°E and (c) 56°W. The error bars refer to the 95% interval of the estimations when assuming that the extremes are independent. The black dots and triangles refer to the results obtained with a second integration of 2 400 000 months.

The first point to emphasize is the monotonic decrease of the variance as a function of the time window (Figs. 5 and 6) for most of the grid points. This behaviour is expected when dealing with variables whose values are bounded (see eq. 12 for ξ positive). One remarkable point is located at (47°N, 135°E) at 350 hPa for which the variance first increases for small values of the time window and then slowly decreases. Another remarkable behaviour is found at 53°N and 135°E at 350 hPa for which, the variance first decreases and then increases up to $n = 600$ months. The latter behaviour has an important implication for the 'predictability' of the extremes since the uncertainty on the extreme values is increasing at these locations and suggests further that a Fréchet type distribution would be adopted for a certain range of time windows.

One can also remark that at 350 hPa, the variance of the extremes is rapidly decreasing over the continental region (50°E up to 135°E) at low latitudes (30° up to 42° North) at the entrance

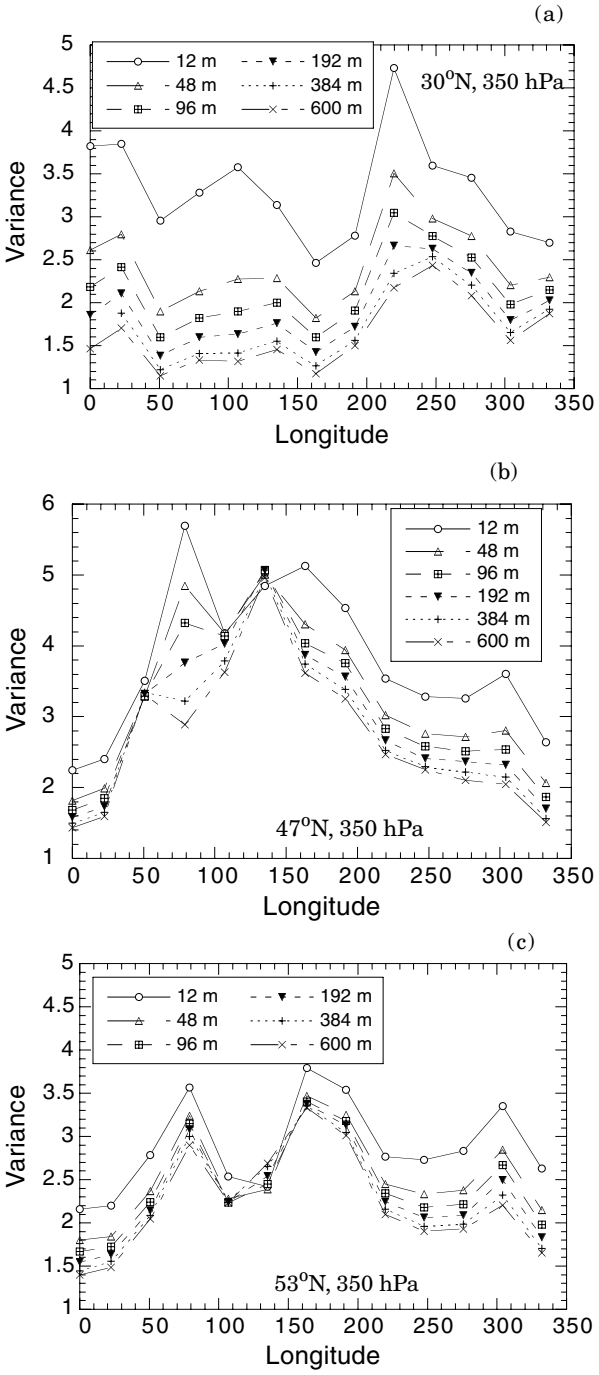

Fig. 5. Spatial dependence of the variance of the (experimental) extreme value distribution at 350 hPa for different time windows along the parallels (a) 30°N, (b) 47°N and (c) 53°N.

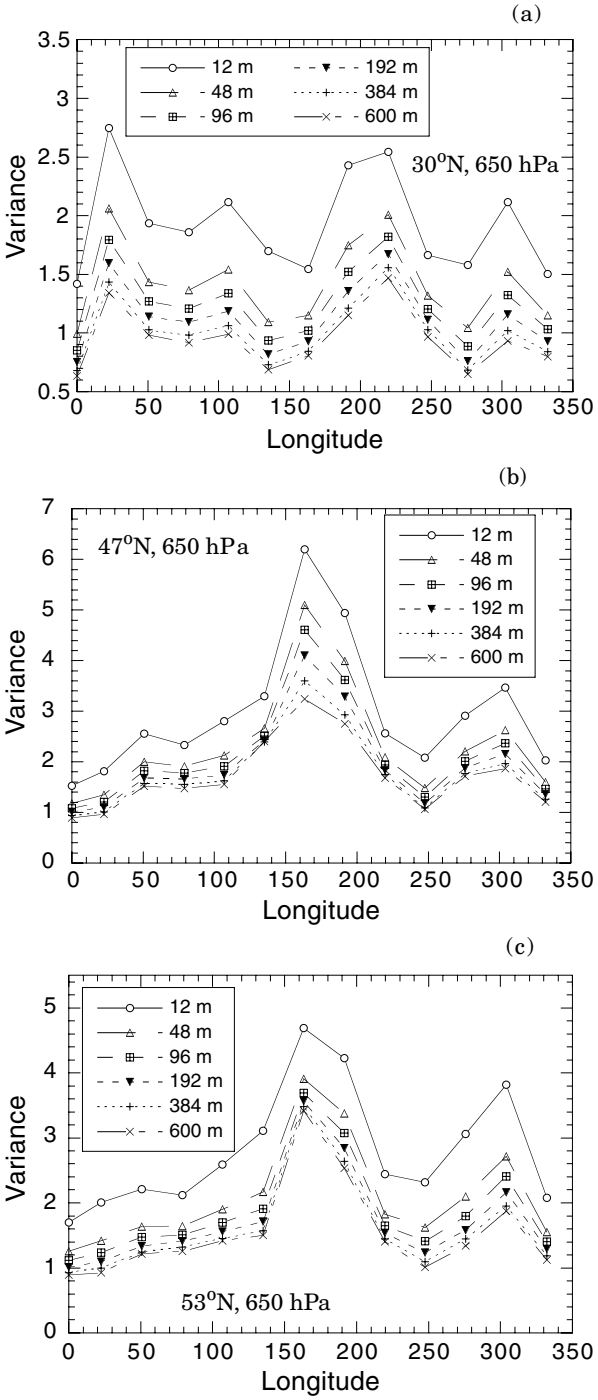

Fig. 6. As in Fig. 5 but at 650 hPa.

of the pacific storm track. For 650 hPa, this rapid decrease is located farther east between 150°E and 200°E, in the pacific region of high baroclinic activity (or dynamical instability). Note also that at low latitudes the variance of the extremes becomes much more uniform as the time window is increased. This trend is less clear for higher latitudes (47°N and 53°N).

Similarly, the skewness parameter is increasing quite homogeneously with the time window at all the longitudes for the lower latitudes (first panels of Figs 7 and 8) and the two levels, up to a value close to 0.9 for a time window of 600 months (corresponding to a value of ξ close to 0.05). For the higher latitudes, the behaviour is much less homogeneous in space with alternating regions of increasing and decreasing skewnesses that

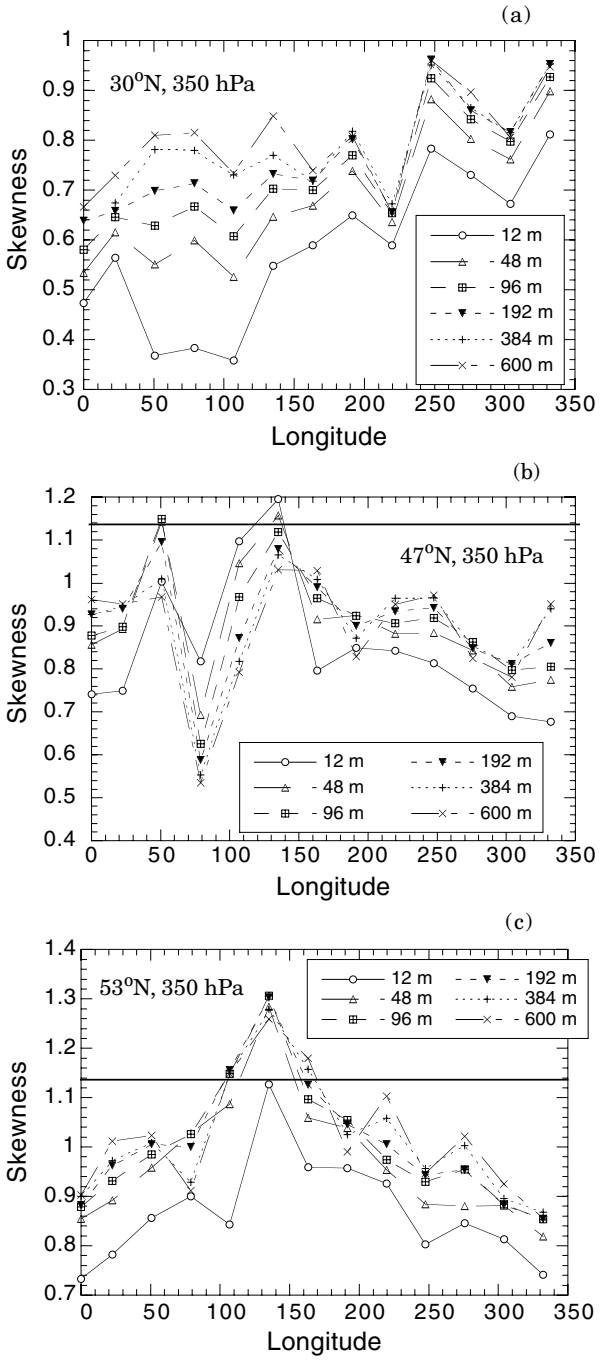

Fig. 7. As in Fig. 5 but for the skewness parameter. The thick continuous line indicates the threshold at which one passes from a positive shape parameter, κ, to a negative one.

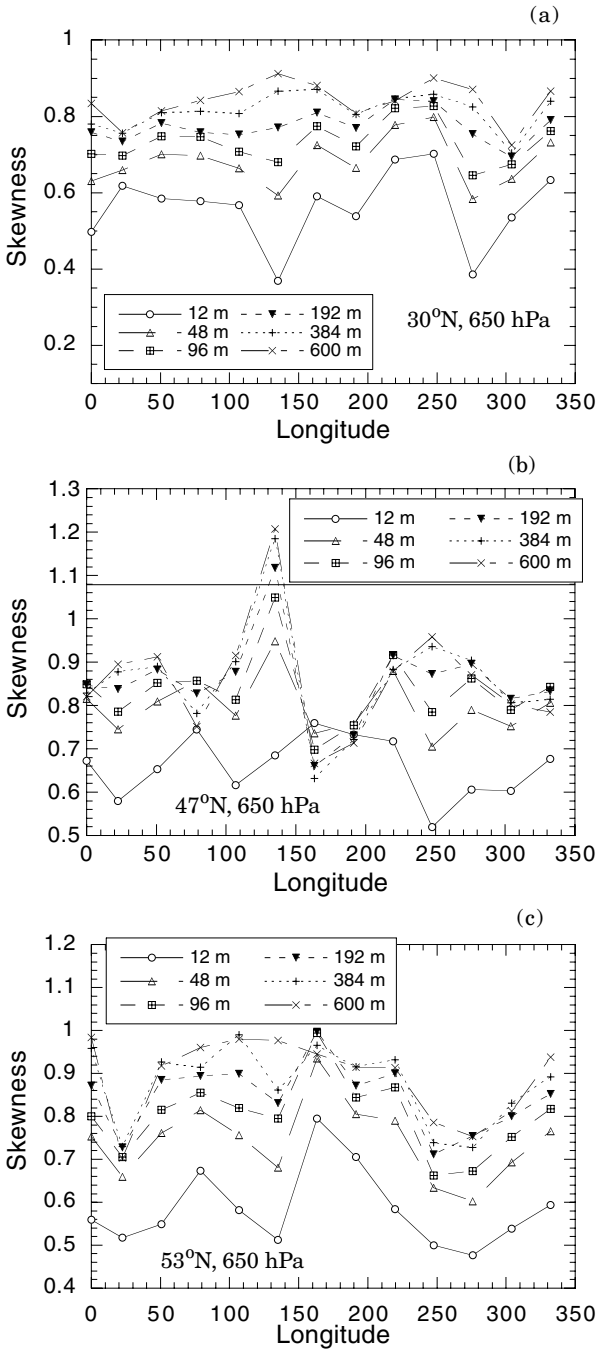

Fig. 8. As in Fig. 7 but at the 650 hPa level.

could be much larger than the value corresponding to the gumbel distribution.

4.2. Model checking and inference

To evaluate the quality of the fit, different tools have been developed that falls into two main categories. First the graphical techniques that essentially compares empirical and model-derived quantities and second, the goodness of fit tests like the Kolmogorov–Smirnov test. In the present section, we will only focus on the first ones since they already provide the information we are interested in. Two traditional graphical representation are used here, the so-called Quantile plot and the Return level plot. The first one consists in representing the empirical and model quantiles,

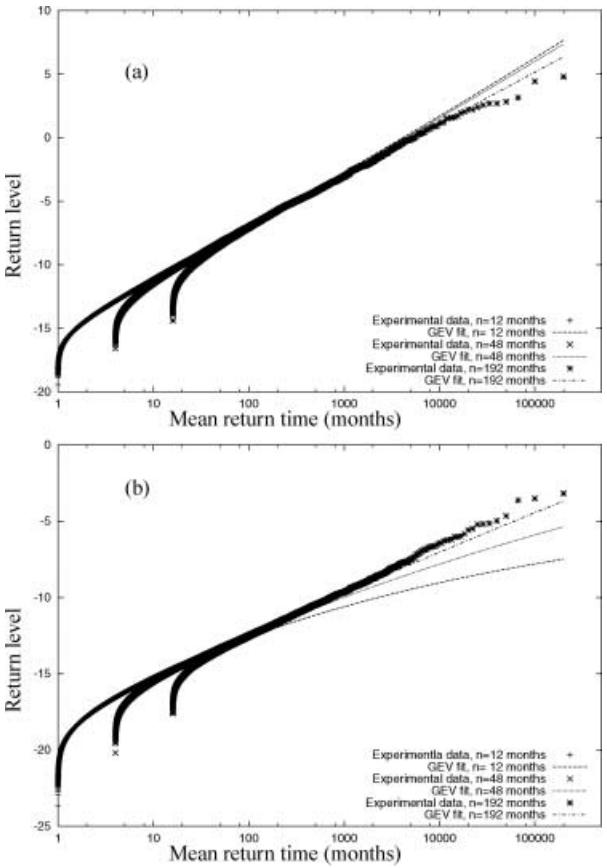

Fig. 9. Return level plot as obtained for 3 different time windows at grid point (47°N, 135°E) and level (a) 350 hPa and (b) 650 hPa.

$$\{[G^{-1}(i/(n+1)], z(i), i = 1, \ldots, n\}, \tag{20}$$

where G is the GEV distribution fitted to the data and $z(i)$ are the ordered maxima such that $z(i-1) \leq z(i)$. The second one consists to plot first the model quantiles as a function of the return period $T = 1/(1 - i/(n+1))$ and to represent on the same plot the empirical quantiles $z(i)$.

For illustrative purposes the return period computed for different time windows at grid point (47°N, 135°E) for (a) the 350 hPa level and (b) the 650 hPa level is depicted in Fig. 9, using the parameters α_p, β_p and ξ already evaluated by means of the L-moment technique (see e.g. Stedinger et al., 1993). In the first case, the return period computed for the different windows are quite similar for large values of T and the fits are close to the experimental data. On the other hand, for the lower level, the differences between the return period are marked in accordance with the very different skewness parameters found for these time windows. It is also interesting to note that the model fits are far from the empirical data for small time windows. The model inadequacy at 650 hPa for small time windows is also apparent in the Quantile plot (Fig. 11b) while the fit

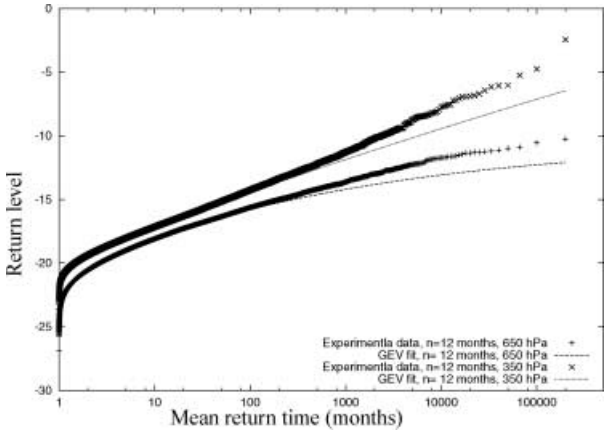

Fig. 10. Return level plot for a window of 12 months at grid point (53°N, 135°E) for both levels.

looks much better at 350 hPa (Fig. 11a). From the latter figure it is clear that a very good fit is reached for a time window of $n = 480$ months. It is interesting to point out that the improvement of the quality of the fit is concomitant with the convergence of the skewness and shape parameters shown in Figs. 2 and 4.

For 650 hPa, the large discrepancy appearing in the fitted and empirical curves would suggest that low extremes pertains to different physical phenomena than large extreme values, as it has already be postulated by several authors in different context (see Van den Brink et al., 2004, and references therein). For instance, Van den Brink et al. (2004) have found such type of mixed distribution for wind events and they have associated the presence of the second population (very rare events) with the merging of successive cyclones. Although such an approach seem to be applicable for the results shown in Fig. 9b, one must stress that two populations are sometimes not enough as illustrated in Fig. 10, where the return level plot is shown for the data recorded at the two levels for grid point 53°N, 135°E and a window $n = 12$ months.

To summarize, the quality of the GEV fit is concomitant with the convergence of the skewness and shape parameters towards a plateau. For most of the grid points, it is reached for time windows of the order of 120 and 240 months. But in some regions, the negative shape parameter for large windows suggest that the asymptotic distribution is not reached yet. The fact that for short time windows (of the order of 12 months) this convergence is not completed does not preclude the possibility to fit (one or several) GEV distributions to the data. But the absence of a clearcut convergence raises some doubts on the inference of the return level of very rare events.

5. Spatial characteristics of the extremes

Up to now, we have demonstrated the slow convergence of the distribution of the extremes of the temperature in the QG model

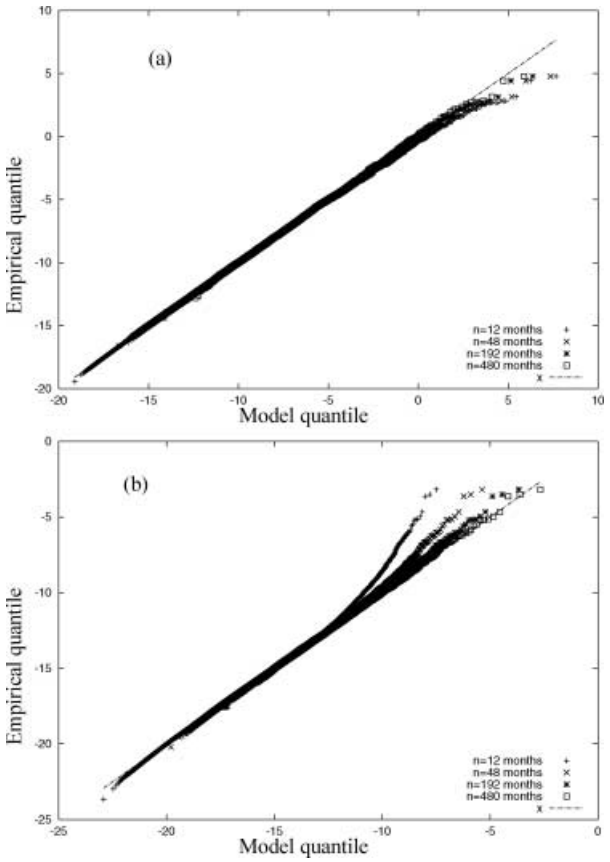

Fig. 11. Quantile plot as obtained for four different time windows at grid point (47°N, 135°E) and level (a) 350 hPa and (b) 650 hPa.

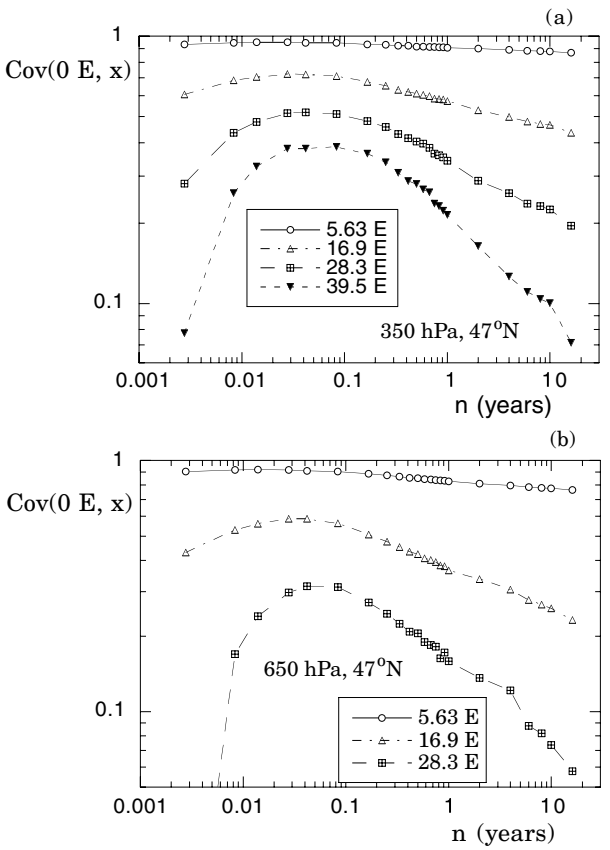

Fig. 12. Covariance between the extremes recorded at different grid points as a function of the time window, *n*. The reference point is (47°N, 0°E). (a) 350 hPa and (b) 650 hPa.

towards the Weibull type distribution expected for bounded systems. This of course implies that the asymptotic distribution of multivariate temperature extremes (as presented in Coles, 2001) cannot be reached either for the typical windows used here, since the marginal distributions have to be given by one of the universality classes. This evidence precludes the possibility to use with confidence the limit classes deduced from the multivariate theory. However, some information on the spatial properties of the extremes can still be extracted from the data. In particular, the spatial dependences can be deduced directly from eqs (13)–(16) based on the *empirical* distributions. This analysis will allow us to evaluate the possibility to factorize the multivariate distribution into the (empirical) marginal distributions computed at each location.

A first analysis that should be performed to clarify the spatial properties of the extremes is to evaluate the linear dependence through the covariance. Figure 12 shows the evolution of the covariance between the grid point located at 47°N 0°E and four other points located on the same parallel at 5.63°E, 16.9°E, 28.3°E, 39.5°E, respectively. Two remarkable features should be emphasized. First, the covariance increases for short time windows. Afterwards, the covariance decreases slowly for increasing *n*. The maximum value is attained at about 5–15 d for points close to each other while a bit later for points that are far.

To interpret this behaviour, one must first recognize that once one selects a window *n*, one selects a domain size over which synoptic scale and (non-stationary) planetary scale perturbations can propagate. On one hand, if *n* is small the distance of advection of the perturbation associated (in particular) with an extreme event is small and will only affect close points during this time window. For larger *n*, this perturbation could propagate on longer distances and therefore introduce correlations between extremes recorded during the period *n* at sites located far apart. On the other hand, for very large values of *n*, several perturbations producing local extreme events can pass through both locations during the period n and the selection will highly depend on the local predominance of one extreme event on another. In this case, the correlation should be smaller. Between these limiting values of *n*, a maximum in the correlation should be reached linked to the typical timescale of propagation of the perturbations between the two sites considered.

It is worth mentioning that this picture is valid for dynamical modes that are propagating in space. For stationary waves, this

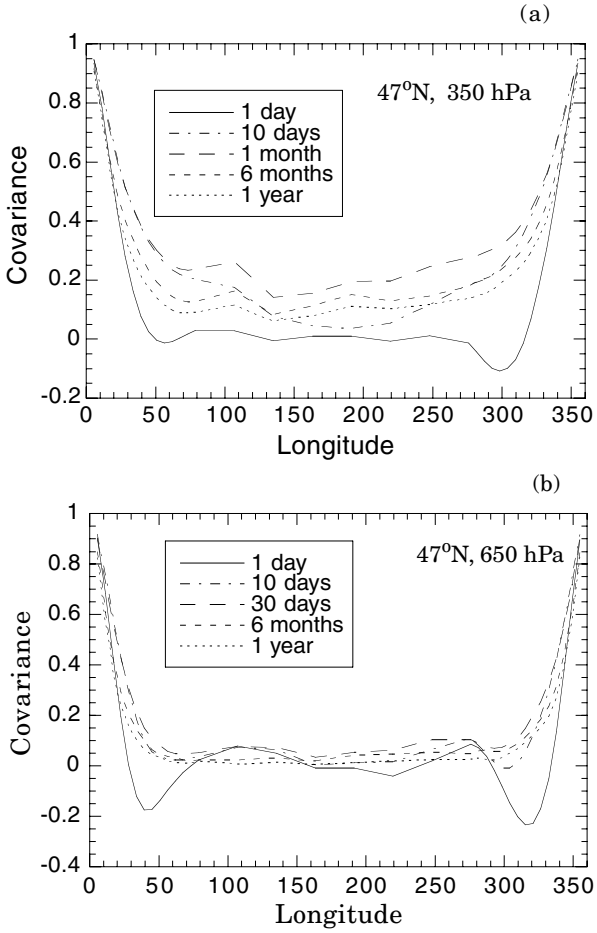

Fig. 13. Spatial dependence of the covariance between the extremes for different time windows, n. The reference point is (47°N, 0°E). (a) 350 hPa and (b) 650 hPa.

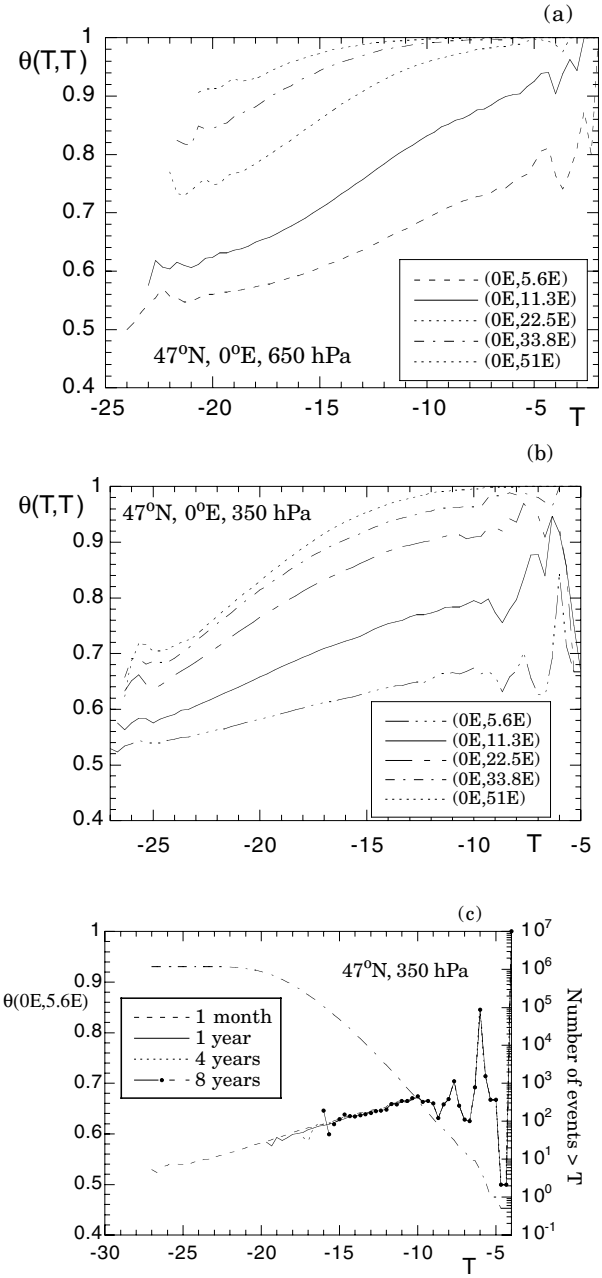

Fig. 14. The amplitude of θ, measuring the interdependence of extremes, as a function of the threshold temperature, T, for grid point (47°N, 0°E) at (a) 650 hPa and (b) 350 hPa. The different curves correspond to extremes recorded at different distance from the reference point. (c) θ for grid points located at (47°N, 0°E) and (47°N, 5.6°E) for different time windows n. The dash-dotted line represents the number of extreme events larger than T.

description does not hold and the possible correlations between regions will depend only on the length scale associated with these waves. As we will see below, quasi-stationary "topographically forced" waves should play a role for low maximum values.

Figure 13 displays the spatial dependence of the covariance for different time windows at 47°N. The reference point is 0°E. For both levels, the correlation is varying with the time window n in a way already discussed above. It is however interesting to emphasize an important difference between the two levels: at 350 hPa, the covariance becomes positive for all distances from the reference point, while for 650 hPa, this covariance is close to 0 between 50°E and 50°W for all the time windows, suggesting the independence for large distances. Note however that the covariance for monthly maxima displays two small local maxima around 100° and 250° Est. The spatial dependences of the extremes are further investigated using the measures discussed in Section (2.2).

First, the parameter $\theta(T, T)$ is computed for different values of the threshold T and for all bivariate combinations of locations for monthly maxima. Figures 14a and 14b display the variation of θ as a function of T at both levels for various combinations of locations along the 47°N parallel. For comparison, one of the locations is fixed and used as a reference (0°E). θ is clearly increasing with T, indicating that large extreme values are less

dependent to the extreme amplitude at other locations than small extremes. In addition, the closest points display a dependence whatever is the quantile value (θ never reached 1). For distant points the curves saturate to 1 for large T, but is smaller than one for smaller quantile values. This suggests that small extreme values are interdependent even if they are occurring far apart. This picture for a specific (large) threshold is not substantially modified with the change of time window, as revealed in Fig. 14c. Note that the fluctuations appearing at the end of the curves are associated with the rapid decrease of the number of events recorded for large T (see dash-dotted line in Fig. 14c).

A summary of the spatial dependence θ of the monthly maxima for different locations and different thresholds is shown in Fig. 15. Each panel shows θ as a function of the longitude. The value $\theta = 0.5$ locates the reference point used in each panel. The different curves correspond to a selection of threshold values, T. One prominent feature of these graphs is that θ does not display a monotonic increase as a function of the distance from the reference point. Some secondary minima are present, suggesting the presence of teleconnections between the extremes in space. For points located over the East part of the Atlantic (panels a and f) important interdependences are visible with Central Asia and Central North America. Panel e with the reference point located over North America reflects the same dependence. For points located over the Pacific region, teleconnections with the West Atlantic are present (panel d). A weak teleconnection between Central North America and East Asia is also found (panel c). For larger time windows, the dependences are similar except that one is only left with the upper curves closer to 1, as suggested by the results of Fig. 14c. At 350 hPa, the long-distance spatial dependence display the same trend as a function of the threshold but is much more homogeneous in space (Fig. 15b).

The long-range interdependences of small maximum values at both levels suggest that they are associated with planetary scale flow anomalies that coherently affect large domains. This in turn suggests that large maxima are rather associated with the baroclinic activity whose space scales are smaller. In addition, the specific teleconnection pattern found at 650 hPa for low extreme values is strongly correlated with the land-sea contrast and the topography, suggesting the crucial role played by quasi-stationary topographically-forced planetary modes known to be present in atmospheric flows (see e.g. Tung and Lindzen, 1979; Shepherd, 1987; Malguzzi et al., 1996).

As already mentioned in Section (2.2), the measure based on θ compares local extremes based on different quantiles of the respective marginal distributions. The second measure, $\xi(u)$, presented in Section (2.2) allows to avoid this problem. Figure 16 shows the result for several quantile values of the

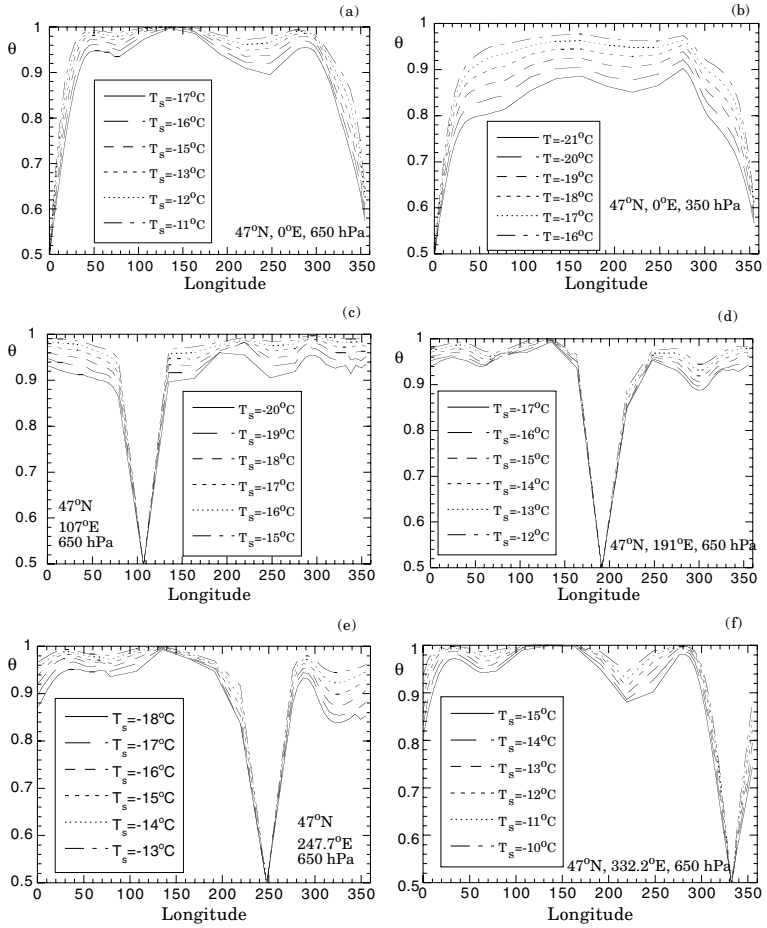

Fig. 15. Spatial dependence of θ for (a) the reference grid point (47°N, 0°E) at 650 hPa and (b) at 350 hPa. Panels (c), (d), (e) and (f) correspond to other reference points, (47°N, 107°E), (47°N, 191.4°E), (47°N, 247.7°E) and (47°N, 332.2°E), respectively. The different curves in each panel correspond to different temperature thresholds.

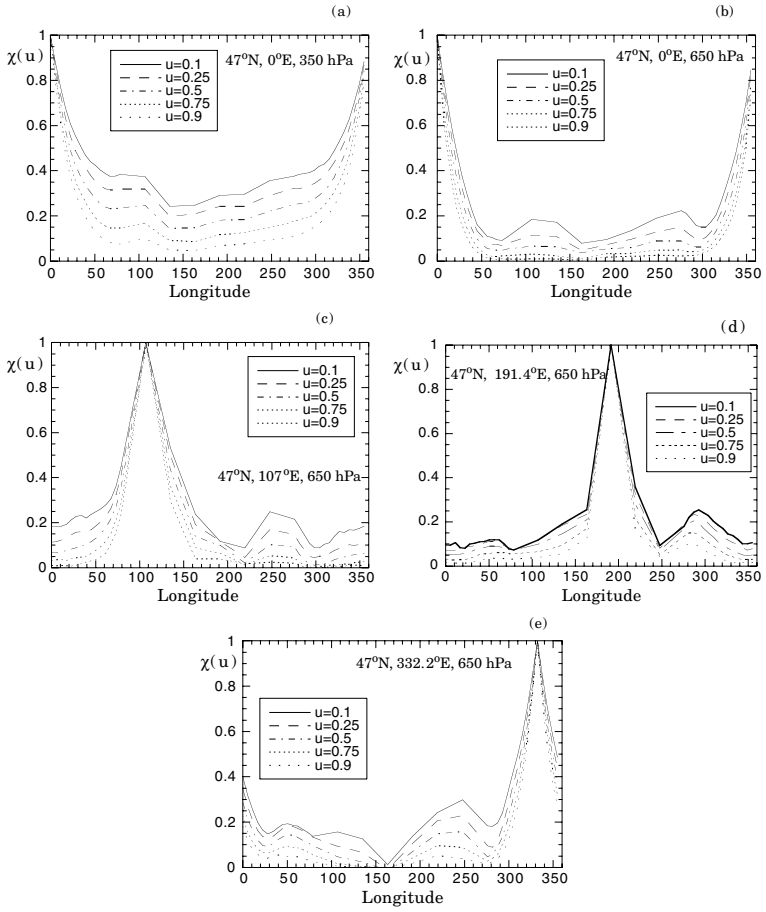

Fig. 16. Spatial dependence of $\xi(u)$ for (a) the reference grid point (47°N, 0°E) at 350 hPa and (b) at 650 hPa. Panels (c), (d), (e) correspond to other reference points, (47°N, 107°E), (47°N, 191.4°E) and (47°N, 332.2°E) at 650 hPa, respectively. The different curves in each panel refer to different quantile thresholds.

uniform variates U and V. Note that the smaller the value of this measure, the smaller is the dependence between the extremes. Clearly, the teleconnections with central Asia and Central North America are still present at 650 hPa suggesting that the results obtained in Fig. 15 are not an artefact associated with the differences of quantile values of the respective marginal distributions.

These teleconnections also display a dependence as a function of the latitude as illustrated in Fig. 17. For lower latitudes, the teleconnections at 650 hPa tend to disappear while for higher latitudes to be reinforced. At 350 hPa, teleconnections similar to the ones obtained at 650 hPa appear for higher latitudes, suggesting the increasing effect of the model topography on the properties of the extremes at this level.

Most of the work found in the litterature were devoted to the analysis of the teleconnections between the (local) extremes and the underlying meteorological situation at the origin of its occurrence (Gershunov and Barnett, 1998; Yiou and Nogaj, 2004; Cassou et al., 2005). In the present section, we have demonstrated that teleconnections exist between the extremes themselves. This feature suggests that the notion of independence between extreme events should not be adopted as a rule.

6. Conclusions

We have investigated the properties of the temperature maxima of a very long time integration of a Quasi-Geostrophic deterministic model. One finding is the slow convergence (if any) of the moments (and of the shape parameter) of the extreme value probability density function towards asymptotic values. In view of the works already done in low-order deterministic chaotic systems, we attribute this feature to the deterministic character of the underlying dynamics. A similar slow convergence is found in a baroclinic low-order atmospheric model (Charney and Straus, 1980) displaying chaos, suggesting further the relevance of our results. Still the mathematical problem of convergence for continuous time deterministic systems is open and is worth investigating in the future.

These findings have important implications for the extrapolation of the return times of very rare temperature maxima of the model, since they are based on an accurate estimate of the GEV parameters under hypothesis of the convergence of the extreme value distribution towards one of the asymptotic universality classes. Similar results have been obtained with the temperature minima. Note that techniques were developed to speed up

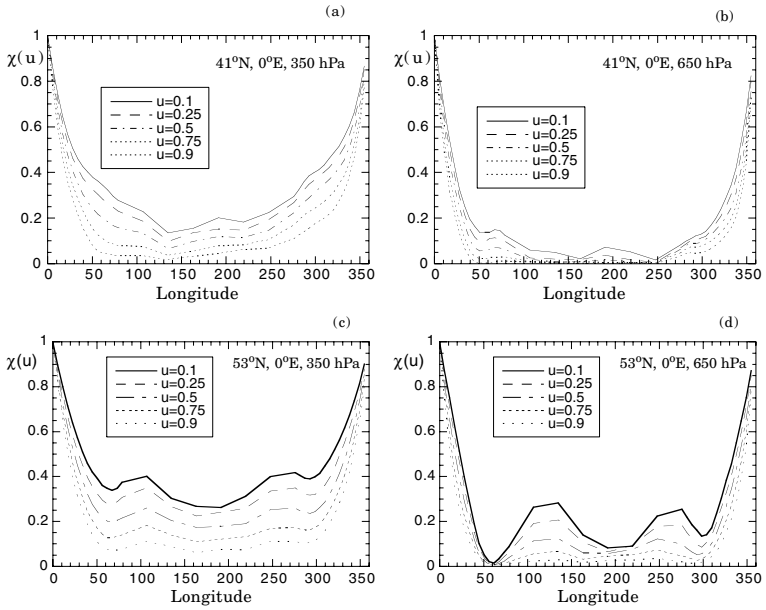

Fig. 17. (a) and (b) as in Fig. 16a and 16b, but for latitude 41°N; (c) and (d) as in Fig. 16a and 16b, but for latitude 53°N.

convergence based on the transformation of the variables and were used recently on wind data (Van den Brink et al., 2004). The application of the latter approach by these authors was possible thanks to the particular probability density of wind data. The impact of such an approach in the context of the present model and in low-order chaotic systems is worth investigating in the future.

The results discussed here cannot of course be directly translated to the real atmosphere and climate, altough the model display a very realistic northern winter climatology at middle latitudes. Further analyses should be performed in more realistic models in order to corroborate our results. But still it provides some important indications on the ability of the GEV distribution to represent the temperature extremes in atmospheric models.

In the second part of this paper, the emphasis has been placed on the spatial dependence of the extremes. First the covariance between maxima located at different sites over the globe increases with the time window up to a timescale associated with the propagation of the perturbation at the origin of the extreme event over the distance between these sites. Beyond this maximum, the spatial covariance is slowly decreasing with the time window, revealing that the hypothesis of spatial independence should be adopted with care.

Since linear correlations are not able to capture the full information on the dependence between non-linearly coupled variables, two alternative measures based on the probability distribution of the extremes have been used. Spatial teleconnections between extremes not clearly apparent with the covariance measure, are found. One particularly interesting feature is the presence of important interdependences between low maximum values located over the Pacific and the West part of the Atlantic, and between the West part of Europe, Central Asia and Central North America. In view of the strong resemblance of this pattern with the land-sea distribution, we suggest that these teleconnections should be related to the the dynamics of quasi-stationary (topographically-forced) planetary waves.

These teleconnections are obtained in the context of a model living around a stable mean winter climatology. They cannot therefore be attributed to some features related with the changes present in the coupled Ocean–Atmosphere system (see e.g. Gershunov and Barnett, 1998). To that respect, the present experiment should be considered as a 'zero-order' approach, since no changes in the ocean dynamics has been incorporated. The impact of the ocean-atmosphere coupling on the teleconnections between the extremes is an open question that is worth addressing in the future.

7. Acknowledgments

C. Nicolis is gratefully acknowledged for numerous enlightning discussions on the extreme value theory. This work has also benefited from the constructive comments of P. Yiou on an earlier version of the manuscript. This work is partly supported by the European Commission under contract no 12975 (NEST).

References

Balakrishnan, V., Nicolis, C. and Nicolis, G. 1995. Extreme value distributions in chaotic dynamics. *J. Stat. Phys.* **80**, 307–336.

Beersma, J. J. and Buishand, T. A. 2004. Joint probability of precipitation and discharge deficits in the Netherlands. *Water Res. Research* **40**, W12508.

Bell, J. L., Sloan, L. C. and Snyder, M. K. 2004. Regional changes in extreme climate events: A future climate scenario. *J. Climate* **17**, 81–87.

Beniston, M. and Stephenson, D. B. 2004. Extreme climate events and their evolution under changing climatic conditions. *Glob. Planet. Change* **44**, 1–9.

Buishand, T. A. 1984. Bivariate extreme-value data and the station-year method. *J. Hydrol.* **69**, 77–95.

Buishand, T. A. 1989. Statistics of extremes in Climatology. *Statistica Neerlandica* **43**, 1–30.

Cassou, Ch., Terray, L. and Phillips, A. S. 2005. Tropical atlantic influence on European heat waves. *J. Climate* **18**, 2805–2811.

Charney, J. G. and Straus, D. M. 1980. Form-drag instability, multiple equilibria and propagating planetary waves in baroclinic, orographically forced, planetary wave systems. *J. Atmos. Sci.* **37**, 1157–1176.

Coles, S. 2001. *An introduction to statistical modeling of extreme values*. Springer Series in Statistics, Springer, New York, 208 p.

Coles, S., Heffernan, J. and Tawn, J. 1999. Dependence measure for extreme value analyses. *Extremes* **2**, 339–365.

Elomer, Y. B., Yagger, T. H. and Tsonis, A. A. 2006. Estimated return periods for hurricane Katrina. *Geophys. Res. Lett.* **33**, L08704.

Emanuel, K. 2005. Increasing destructiveness of tropical cyclones over the past 30 years. *Nature* **436**, 686–688.

Embrechts, P., Klüppelburg, C. and Mikosch, T. 1997. *Modeling extremal events for insurance and finance*. Springer, New York.

Favre, A.-C., El Adlouni, S., Perreault, L., Thiémonge, N. and Bobée, B. 2004. Multivariate hydrological frequency analysis using copulas. *Water Res. Research* **40**, W01101.

Gershunov, A. and Barnett, T. P. 1998. ENSO influence on intraseasonal extreme rainfall and temperature frequencies in the contiguous United States: Observations and model results. *J. Climate* **11**, 1575–1586.

Gumbel, E. J. 1958. *Statistics of extremes*. Columbia University Press, New York.

Hosking, J. R. M., Wallis, J. R. and Wood, E. F. 1984. Estimation of the generalised extreme-value distribution by the method of probability weighted moments. *Technometrics* **27**, 252–261.

Karl, T. R. and Knight, R. W. 1997. The 1995 Chicago heat wave: How likely is a recurrence? *Bull. Amer. Meteor. Soc.* **78**, 1107–1119.

Kharin, V. V. and Zwiers, F. W. 2000. Changes in the extremes in an ensemble of transient climate simulations with a coupled atmosphere-ocean GCM. *J. Climate* **13**, 3760–3788.

Klein Tank, A. M. G., Peterson, T. C., Quadir, D. A., Dorji, S. Zhou, X., and co-authors. 2006. Changes in daily temperature and precipitation extremes in Central and South Asia. *J. Geophys. Res.* **111**, D16105.

Kunkel, K. E., Pielke, R. A. and Changnon, S. A. 1999. Temporal fluctuations in weather amd climate extremes that cause economic and human health impacts: A review. *Bull. Amer. Meteor. Soc.* **80**, 1077–1098.

Malguzzi, P., Speranza, A., Sutera, A. and Caballero, R. 1996. Nonlinear amplification of stationary Rossby waves near resonance. Part I. *J. Atmos. Sci.* **53**, 298–311.

Marshall, J. and Molteni, F. 1993. Toward a dynamical understanding of planetary-scale flow regimes. *J. Atmos. Sci.* **50**, 1792–1818.

Meehl, G. A., Zwiers, F., Evans, J., Knutson, T., Mearns, L., and co-authors. 2000. Trends in extreme weather and climate events: Issues related to modeling extremes in projections of future climate changes. *Bull. Amer. Meteor. Soc.* **81**, 427–436.

Naveau, Ph., Nogaj, M., Ammann, C., Yiou, P., Cooley, D., and co-authors. 2005. Statistical analysis of climate extremes. *C. R. Geosciences Acad. Sci.* **337**, 1013–1022.

Schär, Ch. et al 2004. The role of increasing temperature variability in European summer heatwaves. *Nature* **427**, 332–336.

Shepherd, T. G. 1987. A spectral view of nonlinear fluxes and stationary-transient interaction in the atmopshere. *J. Atmos. Sci.* **44**, 1166–1178.

Sneyers, R. 1979. L'intensité et la durée maximale des précipitations sur la Belgique. Publ. Ser. B, 99, Inst. Roy. Météor. Belgique, 'in French'.

Sparks, J., Changnon, D. and Starke, J. 2002. Changes in the frequency of extreme warm-season surface dewpoints in Northeastern Illinois: Implications for cooling-system design and operations. *J. Appl. Meteor.* **41**, 890–898.

Stedinger, J. R., Vogel, R. M. and Foufoula-Georgiou, E. 1993. Frequency analysis of extreme events. In: *Handbook of Hydrology*, (ed.D. R. Maidment), McGraw-Hill, New-York, pp. 18.1–18.66

Tung, K. K. and Lindzen, R. S. 1979. A theory of stationary long waves. Part I: A simple theory of blocking. *Mon. Wea. Rev.* **107**, 714–734.

Van den Brink, H. W., Können, G. P. and Opsteegh, J. D. 2004. Statistics of extreme synoptic-scale wind speeds in ensemble simulations of current and future climate. *J. Climate* **17**, 4564–4574.

Vannitsem, S. and Nicolis, C., 1997. Lyapunov vectors and error growth patterns in a T21L3 quasi-geostrophic model. *J. Atmos. Sci.* **54**, 347–361.

Yiou, P. and Nogaj, M. 2004. Extreme climate events and weather regimes over the North Atlantic: when and where?. *Geophys. Res. Let.* **31**, L07202.